Electrochemistry Communications 68 (2016) 19–22

Contents lists available at ScienceDirect

Electrochemistry Communications

journal homepage: www.elsevier.com/locate/elecom

# Photo-electrochemical hydrogen sulfide splitting using $Sn^{IV}$-doped hematite photo-anodes

F. Bedoya-Lora *, A. Hankin, G.H. Kelsall

*Department of Chemical Engineering, Imperial College London, South Kensington, London SW7 2AZ, UK*

ARTICLE INFO

*Article history:*
Received 23 March 2016
Received in revised form 17 April 2016
Accepted 18 April 2016
Available online 21 April 2016

*Keywords:*
Hydrogen sulfide
Hematite
Photo-anode
Polysulfide
Photo-electrochemistry
Water splitting

ABSTRACT

Spray-pyrolysed $Sn^{IV}$-doped α-$Fe_2O_3$ photo-anodes were used for photo-assisted splitting of $HS^-$ ions in alkaline aqueous solutions, producing polysulfide ($S_n^{2-}$) ions together with hydrogen at the cathode. Subsequent aerial oxidation of polysulfide could be used to produce elemental sulfur. At an applied electrode potential of 1.07 V (RHE) and an irradiance of 5.6 kW $m^{-2}$, stable photocurrents of ca. 11 A $m^{-2}$ ($2 \times 10^{-3}$ A $W^{-1}$) were recorded over 75 h, polysulfide concentrations increasing linearly with time. Despite being predicted thermodynamically to form iron sulfide(s) in sulfide solutions, such photo-anodes appeared to be stable. In comparison with conventional water splitting under alkaline conditions, the coupled processes of hydrogen sulfide ion oxidation and water reduction had a lower energy requirement.



## 1. Introduction

Research on water splitting with solar energy to produce hydrogen (and oxygen) has focused mainly on synthesis, fabrication, and performance determination of photon-absorbing materials as prospective photo-electrodes at laboratory scale. Thermodynamically less energy-intensive processes such as hydrogen sulfide splitting remain as a concept for lack of suitable semiconductors. Whereas a conventional (liquid) water splitting reactor requires a standard equilibrium potential difference of 1.23 V (1.48 V thermo-neutral potential) to produce oxygen and hydrogen, the corresponding value for hydrogen sulfide splitting into hydrogen and polysulfides is predicted to be only ca. 0.27 V in alkaline solutions, as shown in Fig. 1.

Hydrodesulfurisation uses hydrogen to remove sulfur as $H_2S$ from petroleum products in oil refineries, at which >70 Mt per annum elemental sulfur is produced subsequently by Claus processes [1]. After absorption of $H_2S$ in alkaline solutions, photo-electrochemical splitting of the resulting $HS^-$ ions could form the basis of a more elegant process, producing hydrogen for hydrodesulfurisation and partially oxidising the sulfide to polysulfides, for subsequent oxidation to elemental sulfur in an external reactor. This was addressed decades ago with limited progress [2–5], but regained attention [6–8] as oil refineries produced increasing quantities of $H_2S$. A theoretical maximum of 26% exergy efficiency can be achieved for hydrogen sulfide splitting [9], but again a stable, inexpensive, and efficient photo-electrode material is needed presently. Furthermore, the simultaneous presence of several polysulfide species, predicted by Fig. 1, and their spontaneous oxidation in oxygenated electrolytes still represent a challenge for the measurement of time-dependent electrochemical oxidation efficiencies and individual polysulfide concentrations [10].

Hematite has been the subject of extensive research on water splitting for hydrogen production, mainly because of its stability, low cost, and facile fabrication in thin film form. However, the energy of its conduction band edge precludes spontaneous water splitting and it exhibits low energy conversion efficiencies, impeding scaling up. Recently, interest in hematite as a prospective photo-anode has been rekindled by morphology modification [11], doping, and under-layer deposition [12,13].

We report below results for photo-assisted splitting of $HS^-$ ions in alkaline aqueous solutions using spray-pyrolysed $Sn^{IV}$-doped α-$Fe_2O_3$ photo-anodes, which surprisingly exhibited apparent stability and significant activity, despite being predicted thermodynamically to form iron sulfide(s) in such solutions.

If a photo-electrochemical reactor is used with a single photo-anode, hydrogen sulfide splitting can be summarised in three processes in the semiconductor, photo-anode, and cathode, respectively:

$$(2n-2)\left(Fe_2O_3 + h\nu \underset{\text{recombination}}{\overset{\text{absorption}}{\rightleftharpoons}} Fe_2O_3\left(h^+_{VB}, e^-_{CB}\right)\right) \quad (1)$$

* Corresponding author.
*E-mail address:* f.bedoya-lora13@imperial.ac.uk (F. Bedoya-Lora).

http://dx.doi.org/10.1016/j.elecom.2016.04.010

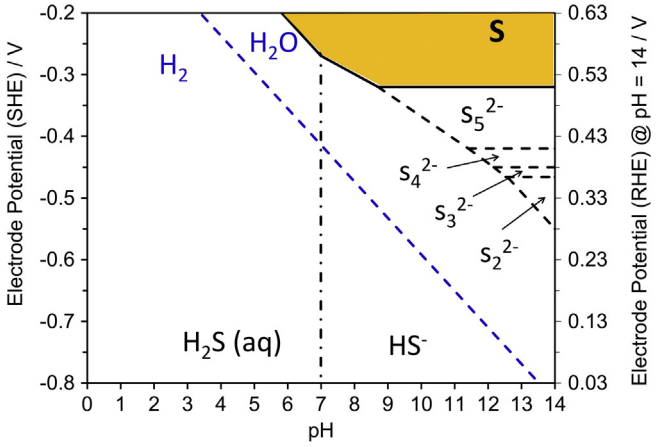


**Fig. 1.** Potential-pH diagram for meta-stable S-$H_2O$ system with all sulfoxy species excluded and dissolved sulfur concentration of 0.5 M.

$$nHS^- + nOH^- + (2n-2)h^+_{VB} \rightarrow S_n^{2-} + nH_2O \quad (2)$$

$$(2n-2)H_2O + (2n-2)e^-_{CB} \rightarrow (n-1)H_2 + (2n-2)OH^- \quad (3)$$

## 2. Materials and methods

### 2.1. $Sn^{IV}$-doped α-$Fe_2O_3$ photo-anodes

$Sn^{IV}$-doped iron oxide was spray pyrolysed at 480 °C onto titanium foil substrates [14], which had been polished with aqueous dispersions of <300 nm alumina particles, degreased with acetone and left overnight in 0.5 M oxalic acid to minimise the oxide layer thickness, rinsed again with acetone and ultra-sonicated in de-ionised water.

0.1 M $FeCl_3$ (Sigma–Aldrich, UK) and 0.6 mM $SnCl_2$ dissolved in ethanol absolute was used as precursor and nebulized with a quartz spray nozzle (Meinhard, US) attached to a CNC machine (Heiz T-720, Germany). 40 layers of precursor solution was sprayed to achieve an estimated thickness of ca. 20 nm [14]. Photo-active areas of fabricated photo-anodes corresponding to the light source's 3 × 6 $mm^2$ beam area, were defined by coating unexposed areas with insulating acrylic lacquer (RS Components, UK).

### 2.2. Photo-electrochemical cell

The photo-electrochemical reactor (PVC body with a quartz aperture) incorporated a Nafion 424 PTFE-reinforced cation-permeable membrane (DuPont Inc.), a $Sn^{IV}$-doped α-$Fe_2O_3$ photo-anode working electrode, and a platinized titanium mesh counter electrode. A HgO|Hg reference electrode was used when electrodes were immersed in 72 $cm^3$ of 1 M NaOH (pH 13.6), while an $Ag_2S$|Ag electrode was used in 1 M NaOH + 0.5 M $Na_2S$ (pH 14) solutions; the catholyte was 88 $cm^3$ of 1 M NaOH (pH 13.6). In the data presented, all electrode potentials were converted to the reversible hydrogen electrode (RHE) scale. The photo-response was monitored under illumination from a Xenon arc lamp (LOT-Oriel) with an intensity of ca. 5.6 kW $m^{-2}$.

Electrolyte solutions were purged in both compartments with high-purity nitrogen for 1 h prior to and during photo-electrolysis, to avoid oxidation of polysulfides by the presence of any adventitious dissolved oxygen. A fixed potential of 0.9 V vs. $Ag_2S$|Ag (1.07 V (RHE)) was applied under illuminated conditions.

### 2.3. Polysulfide concentration determination

UV–visible spectrophotometry (HP 8452 A, Agilent Technologies, UK) was used to quantify polysulfide concentrations, expressed as $S_2^{2-}$ ions, following a previous report [15], but without the need for dilution. A calibration curve was obtained after dissolving elemental sulfur in de-oxygenated 1 M NaOH + 0.5 M $Na_2S$ ($(n-1)'S' + HS^- + OH^- \rightarrow S_n^{2-} + H_2O$) and measuring absorbances at 295 nm. All solutions were kept closed or purged constantly with high-purity nitrogen when possible.

Using an $Ag_2S$|Ag reference electrode and platinum foil working electrode, open circuit potentials of the polysulfide solutions were also measured as a function of concentration.

## 3. Results and discussion

Homogeneous ca. 20 nm thick, brown-red α-$Fe_2O_3$ was spray pyrolysed onto titanium substrates [14,16], producing well-adherent films that appeared chemically stable after being immersed in hydrogen sulfide solution for 4 weeks.

### 3.1. Photocurrent response

Fig. 2 shows typical linear sweep voltammograms for a $Sn^{IV}$-doped α-$Fe_2O_3$ photo-anode in the absence and presence of hydrogen sulfide ions ($HS^-$), under light and dark conditions. The photocurrent onset potential of ca. 0.7 V (RHE) for oxygen evolution in alkaline solution in the absence of sulfide ions ($E_{O_2/OH^-} = 1.229$ V (RHE)) decreased to ca. 0.2 V (RHE) upon addition of $HS^-$ ions. The equilibrium potential (Fig. 1) of the $HS^-$ oxidation reaction (2) to $S_n^{2-}$ ions for $n = 2$:

$$E_{S_2^{2-}/HS^-}\ (\mathrm{RHE})/\mathrm{V} = 0.278 + 0.0296\log(S_2^{2-}) - 0.0592\log(HS^-) \quad (4)$$

combined with its fast kinetics [6], helped to minimise the rates of electron–hole recombination, especially at lower potentials. At a current density of 10 A $m^{-2}$, the photo-potential was ca. 0.4 V (RHE). Photocurrent densities increased rapidly as the potential was increased from 0.87 to 1.07 V (RHE), then reached a plateau just prior to the onset of 'dark' currents at 1.17 V, limited by the photon flux with ultra-band gap energies (> 2.1 eV; λ < 590 nm) and by rates of electron–hole recombination. The latter was determined from measurements of incident photon to current efficiencies, which increased from 4% to 10% at 360 nm in the absence and presence of hydrogen sulfide ions at 1.53 V and 1.17 V (RHE), respectively; hence, less energy was required to achieve higher

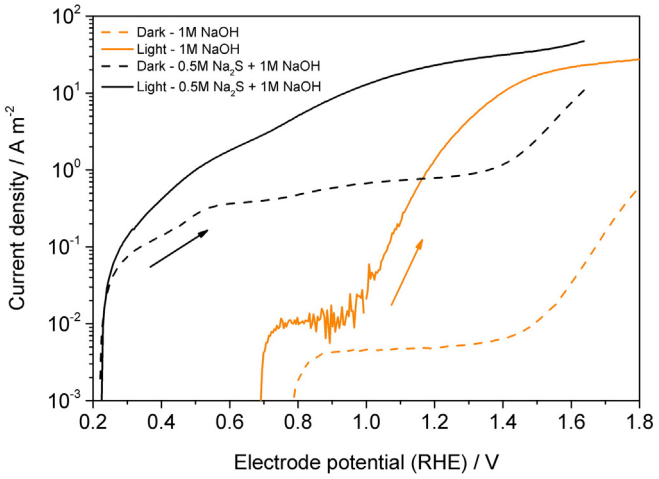


**Fig. 2.** Linear sweep voltammograms for Ti | Sn-doped α-$Fe_2O_3$ | 1 M NaOH ± $Na_2S$ (pH = 14) |Pt | Ti under dark and illuminated conditions; 10 mV $s^{-1}$ scan rate. Xenon Arc lamp irradiance 5.6 kW $m^{-2}$.

photocurrent densities for $HS^-$ oxidation, as clearly evident in Fig. 2. The sharp increase in photocurrent densities at potentials >1.4 V (RHE) in sulfide solutions corresponded to oxidation of sulfides to elemental sulfur, which could be seen as a yellow layer on the photo-anode, especially at potentials ≥1.6 V (RHE), leading to inhibition of the photo-anode reaction.

Fig. 3 shows the time dependence of photocurrent densities at potentials in the range 0.87–1.17 V (RHE). Potentials >1.07 V (RHE) resulted in a minor decrease of photocurrent during the first hour; this was evident only after analysing the $d[j_{photo}]/dt$ gradient over the last 45 min. However, current densities were restored to their initial values after the photo-anode was washed with de-ionised water. This indicated that, despite the predicted instability of α-$Fe_2O_3$ in sulfide solutions, the principal reason for photocurrents decreasing with time was sulfur deposition by the reaction:

$$S_5^{2-} + 2h_{VB}^{+} \rightleftharpoons 5'S' \tag{5}$$

$$E_{S/S_5^{2-}}(\mathrm{RHE})/\mathrm{V} = 0.5084 - 0.0296\log\left(S_5^{2-}\right)$$

### 3.2. Time dependence of polysulfide concentrations

At an applied potential of 1.07 V (RHE), the illuminated $Sn^{IV}$-doped α-$Fe_2O_3$ photo-anode produced photocurrent densities of ca. 11.5 ± 0.5 A $m^{-2}$ over 75 h, after which no sulfur deposit was evident to the naked eye. The resulting time-dependent concentrations of polysulfide ions were determined spectrophotometrically during the first 30 h, using a calibration curve ($r^2 = 0.994$) over the concentration range [0.5–5] mM $S_2^{2-}$. Unlike reported previously [15], dilution was not necessary, though concentrations >20 mM $S_2^{2-}$ generated absorbance values outside the linear response range of the spectrophotometer. Fig. 4 shows the time dependence of polysulfide (expressed as $S_2^{2-}$ ions) concentrations in the anolyte. The concentration of $S_2^{2-}$ ions increased linearly from 3 to 30 h, during which time polysulfide concentrations in the catholyte were less than the detection limit, indicating that their transport from anolyte to catholyte was impeded successfully by the cation-permeable membrane.

Solutions ([0.5–5] mM $S_2^{2-}$) used for spectrophotometric calibration exhibited a similar open circuit potential in sulfide solution with an average of 0.2696 V vs RHE. As reported previously [17], solving the mass balance for sulfur species coupled with Nernst equations for each polysulfide species enabled prediction of their concentrations as a function of potential in the range 0.25–0.55 V (RHE), at pH 14 and at a dissolved sulfur concentration of 0.5 M. Using these particular parameter values, hydrogen sulfide ions ($HS^-$) were expectedly the predominant species, followed by $S_2^{2-}$ ions, accounting for 99.2% of all polysulfide species ($S_n^{2-}$, $n$ = 2–5), justifying their use e.g. in Fig. 4. Kinetics and mechanisms of polysulfide formation will be addressed in a subsequent publication.

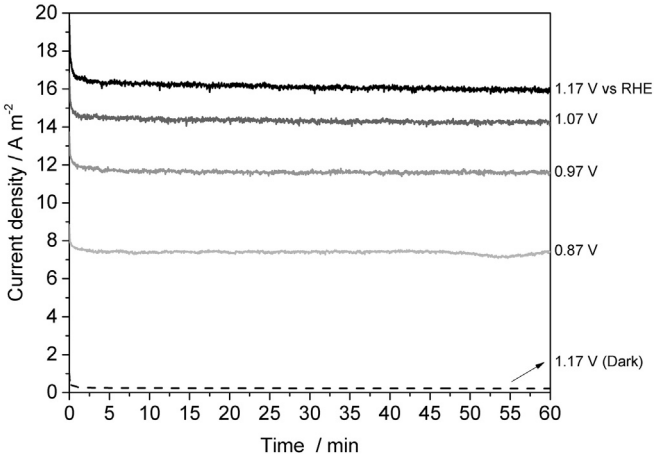


**Fig. 3.** Chronopotentiometry at different potentials for Ti | Sn-doped α-$Fe_2O_3$ | 1 M NaOH + 0.5 M $Na_2S$ | Pt | Ti. Xenon Arc lamp irradiance 5.6 kW $m^{-2}$, pH = 14.

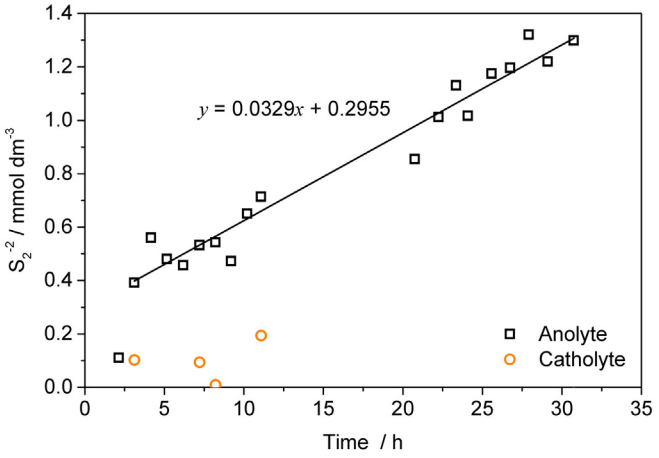


**Fig. 4.** Time dependence of polysulfide (predominantly $S_2^{2-}$) ion concentration produced by illuminated (5.6 kW $m^{-2}$) Sn-doped α-$Fe_2O_3$ photo-anode at 0.9 V vs. $Ag_2S$|Ag (1.07 V (RHE)).

### 3.3. Analysis of charge yields

From the gradient ($d[S_n^{2-}]/dt$) of the regression line in Fig. 4, the charge yield ($\Phi_{S_n^{2-}}^{e}$) for polysulfide production can be estimated for reaction (2) from:

$$\Phi_{S_n^{2-}}^{e} = \frac{V_a \cdot d\left[S_n^{2-}\right]}{dt}\frac{(2n-2)F}{j \cdot A_a} \tag{6}$$

where $V_a$ is the anolyte volume, $A_a$ the photo-anode area, $j$ is the average photocurrent density (11.5 A $m^{-2}$) over time $t$, and $(2n-2)$ is the hole stoichiometry of reaction (2). With the illuminated $Sn^{IV}$-doped α-$Fe_2O_3$ photo-anode at an applied potential of 1.07 V (RHE), $S_5^{2-}$ ions were probably formed at the photo-anode surface (i.e. $n = 5$), but the photo-anode reaction would have been coupled to homogeneous electron transfer reactions, e.g.

$$S_5^{2-} + 3HS^- + 3OH^- \xrightarrow{k_c} 3H_2O + 4S_2^{2-} \tag{7}$$

as predicted by Fig. 1. Importantly, as the best estimate of the flat band potential $U_{FB}$(α-$Fe_2O_3$) ≈ 0.76 V (RHE) (−0.067 V (SHE) at pH 14 [18], even at low photo-anode potentials at which photo-generated electrons could reach the anode | electrolyte interface, those electrons would be insufficiently energetic to reduce the polysulfides by the reverse of reaction (2). Fig. 2 shows how much more facile photo-oxidation of $HS^-$ was than for $OH^-$ ions. Hence, it was reasonable to assume an effective charge yield of unity for $S_n^{2-}$ formation, enabling a mean hole stoichiometry of 3.25 and $n = 2.63$ to be calculated from Eq. (6) for reaction (2) for the conditions corresponding to Fig. 4.

Despite the facile photo-oxidation of $HS^-$ ions on α-$Fe_2O_3$ photo-anodes, they exhibited relatively low incident photon to current efficiencies, typical of their reported behaviour in alkaline conditions [14,19,20]. Unfortunately, an applied bias was still required, as for their use for water splitting, because the potential corresponding to their conduction band edge is insufficiently negative to generate hydrogen spontaneously.

## 4. Conclusions

Photo-assisted oxidation of $HS^-$ to polysulfide ions was achieved using a $Sn^{IV}$-doped α-$Fe_2O_3$ photo-anode with lower photocurrent onset potentials than for $OH^-$ oxidation and achieving greater photocurrent densities that were quite stable over 75 h. $S_2^{2-}$ ions were found to be the predominant polysulfide species for the limited time/conversions tested but would be expected to tend to $S_5^{2-}$ ions in the envisaged technological process. The potential applied to minimise electron–hole recombination kinetics should not exceed (i.e. <1 V (RHE)) the onset of dark current density, to avoid deposition of inhibiting elemental sulfur.

## Conflict of interest

None.

## Acknowledgements

The authors thank Colombia COLCIENCIAS scholarship 568 for PhD studies abroad, supporting a PhD studentship for FB and the UK EPSRC for a Pathways to Impact grant, funding a post-doctoral research associateship for A.H.

## References

[1] Mineral Commodity Summaries 2015, U.S. Geological Survey, U.S. Department of the Interior and U.S. Geological Survey, 2015.
[2] R.C. Kainthla, J.O.M. Bockris, Photoelectrolysis of $H_2S$ using an n-CdSe photoanode, Int. J. Hydrog. Energy 12 (1987) 23–26.
[3] G. Lu, S. Li, Hydrogen production by H2S photodecomposition on $ZnFe_2O_4$ catalyst, Int. J. Hydrog. Energy 17 (1992) 767–770.
[4] S.A. Naman, S.M. Aliwi, K. Al-Emara, Hydrogen production from the splitting of $H_2S$ by visible light irradiation of vanadium sulfides dispersion loaded with $RuO_2$, Int. J. Hydrog. Energy 11 (1986) 33–38.
[5] S.V. Tambwekar, M. Subrahmanyam, Photocatalytic generation of hydrogen from hydrogen sulfide: an energy bargain, Int. J. Hydrog. Energy 22 (1997) 959–965.
[6] V. Preethi, S. Kanmani, Photocatalytic hydrogen production, Mater. Sci. Semicond. Process. 16 (2013) 561–575.
[7] U.V. Kawade, R.P. Panmand, Y.A. Sethi, M.V. Kulkarni, S.K. Apte, S.D. Naik, B.B. Kale, Environmentally benign enhanced hydrogen production via lethal H2S under natural sunlight using hierarchical nanostructured bismuth sulfide, RSC Adv. 4 (2014) 49295–49302.
[8] X. Zong, J. Han, B. Seger, H. Chen, G. Lu, C. Li, L. Wang, An integrated photoelectrochemical–chemical loop for solar-driven overall splitting of hydrogen sulfide, Angew. Chem. 126 (2014) 4488–4492.
[9] R.O. Shamim, I. Dincer, G. Naterer, Thermodynamic analysis of solar-based photocatalytic hydrogen sulphide dissociation for hydrogen production, Int. J. Hydrog. Energy 39 (2014) 15342–15351.
[10] S.A. Khan, UV-ATR spectroscopy study of the speciation in aqueous polysulfide electrolyte solutions, Int. J. Electrochem. Sci. 7 (2012) 561–568.
[11] J.Y. Kim, G. Magesh, D.H. Youn, J.-W. Jang, J. Kubota, K. Domen, J.S. Lee, Single-crystalline, wormlike hematite photoanodes for efficient solar water splitting, Sci. Rep. 3 (2013) (Article number: 2681).
[12] T. Hisatomi, H. Dotan, M. Stefik, K. Sivula, A. Rothschild, M. Grätzel, N. Mathews, Enhancement in the performance of ultrathin hematite photoanode for water splitting by an oxide underlayer, Adv. Mater. 24 (2012) 2699–2702.
[13] F. Le Formal, N. Tetreault, M. Cornuz, T. Moehl, M. Gratzel, K. Sivula, Passivating surface states on water splitting hematite photoanodes with alumina overlayers, Chem. Sci. 2 (2011) 737–743.
[14] C.K. Ong, S. Dennison, S. Fearn, K. Hellgardt, G.H. Kelsall, Behaviour of titanium-based $Fe_2O_3$ photo-anodes in photo-electrochemical reactors for water splitting, Electrochim. Acta 125 (2014) 266–274.
[15] D.L. Pringle, The Nature of the Polysulfide AnionPhD thesis Iowa State University, 1967.
[16] C.K. Ong, Design and Performance of Photo-Electrochemical Reactors with $Fe_2O_3$ Photo-Anodes for Water SplittingPhD thesis Imperial College London, London, 2013.
[17] G.H. Kelsall, I. Thompson, Redox chemistry of H2S oxidation by the British gas Stretford process. Part I: thermodynamics of sulphur–water systems at 298 K, J. Appl. Electrochem. 23 (1993) 279–286.
[18] A. Hankin, J.C. Alexander, G.H. Kelsall, Constraints to the flat band potential of hematite photo-electrodes, Phys. Chem. Chem. Phys. 16 (2014) 16176–16186.
[19] H.K. Mulmudi, N. Mathews, X.C. Dou, L.F. Xi, S.S. Pramana, Y.M. Lam, S.G. Mhaisalkar, Controlled growth of hematite (α-$Fe_2O_3$) nanorod array on fluorine doped tin oxide: synthesis and photoelectrochemical properties, Electrochem. Commun. 13 (2011) 951–954.
[20] L. Wang, C.-Y. Lee, P. Schmuki, Improved photoelectrochemical water splitting of hematite nanorods thermally grown on Fe–Ti alloys, Electrochem. Commun. 44 (2014) 49–53.